Air-Puff-Induced Dynamics of Ocular Components Measured with Optical Biometry

Ewa Maczynska,[1] Jagoda Rzeszewska-Zamiara,[2] Alfonso Jimenez Villar,[1] Maciej Wojtkowski,[1,3] Bartlomiej J. Kaluzny,[2] and Ireneusz Grulkowski[1]

[1]Institute of Physics, Faculty of Physics, Astronomy and Informatics, Nicolaus Copernicus University, Torun, Poland
[2]Division of Ophthalmology and Optometry, Department of Ophthalmology, Collegium Medicum, Nicolaus Copernicus University, Bydgoszcz, Poland
[3]Institute of Physical Chemistry, Polish Academy of Sciences, Warsaw, Poland

Correspondence: Ireneusz Grulkowski, Institute of Physics, Faculty of Physics, Astronomy and Informatics, Nicolaus Copernicus University, Grudziadzka 5, 87-100 Torun, Poland;
igrulkowski@fizyka.umk.pl.

Submitted: January 19, 2019
Accepted: March 25, 2019

Citation: Maczynska E, Rzeszewska-Zamiara J, Jimenez Villar A, Wojtkowski M, Kaluzny BJ, Grulkowski I. Air-puff-induced dynamics of ocular components measured with optical biometry. *Invest Ophthalmol Vis Sci*. 2019;60:1979–1986. https://doi.org/10.1167/iovs.19-26681

Purpose. To analyze the dynamics of all optical components of the eye and the behavior of the eyeball under air-puff conditions in vivo. To determine the impact of the intraocular pressure (IOP) on the air-puff-induced deformation of the eye.

Methods. Twenty eyes of 20 healthy subjects were included in this study. The dynamics of the ocular components, such as the cornea, the crystalline lens, and the retina, was measured by a prototype swept source optical coherence tomography biometer integrated with the air-puff system. The system allows to acquire a series of axial scans at the same location as a function of time with no transverse scanning. Several parameters were extracted from optical coherence tomography data. The IOP was measured using a Goldmann applanation tonometry. The measurements of the eyes were performed before and 2 hours after administration of IOP-reducing drops, namely, 0.2 % brimonidine tartrate.

Results. There is a statistically significant correlation of corneal thickness, vitreous depth, and eye length with IOP. The deformation amplitudes of the cornea and the crystalline lens are inversely proportional to the IOP, but statistical significance is achieved only for the cornea. The crystalline lens is displaced without compression, and the return has the form of wobbling. The reduction of IOP level induces corresponding changes in the extracted parameters.

Conclusions. Optical biometry combined with air puff provides comprehensive information on the in vivo behavior of all ocular components, including the crystalline lens. Measurement of the axial length dynamics of during deformation enables correcting the deformation for eye retraction.

Keywords: intraocular pressure, ocular biometry, optical coherence tomography, ocular dynamics, biomechanics

The eye constitutes the dynamic and complex optical system that enables visual perception. The assessment of the intraocular pressure (IOP) is crucial in the management of glaucoma patients, but the IOP and the viscoelastic (biomechanical) properties of the cornea are coupled, which limits the precision of the IOP measurement.[1,2] A gold standard in the IOP assessment is Goldmann applanation tonometry (GAT), which requires contact of the eye with the prism after instillation of local anesthetic drops and fluorescein to perform static deformation (applanation) of the cornea.[3] IOP data from GAT depend on the curvature and the thickness of the cornea.[4,5] However, the dynamic response of the eye to mechanic excitation is a key for the IOP measurement in modern noncontact tonometers. Mechanic stimulation is usually induced by the air stream formed to short pulse (ca. 20 ms) that deforms the anterior chamber, and the dynamic macroscopic behavior of corneal tissue is analyzed during excitation.[6]

Two types of noncontact air-puff-based tonometers have been developed and approved by the Food and Drug Administration: Ocular Response Analyzer (ORA; Reichert, Inc., Depew, NY, USA) and Corvis ST tonometer (Oculus Optikgeräte GmbH, Wetzlar, Germany). ORA determines corneal response during applanation by an air jet.[7,8] In this technique, the infrared light beam reflected from the cornea is detected by an optoelectronic device. The bidirectional applanation moments are identified and allow one to determine the corneal hysteresis, which is defined as the pressure difference between both applanation instances. The Corvis ST tonometer, in turn, combines a high-speed Scheimpflug camera and an air-puff for visualization and quantitative analysis of the induced corneal deformation.[9–11]

Optical coherence tomography (OCT) is another example of optical modality that can be integrated with an air puff.[12,13] Generally, OCT detects light back-reflected or back-scattered from the structures of the object. Since the first demonstration of OCT over 25 years ago, this imaging method showed its feasibility in visualizing ocular structures, and it became a standard modality in the diagnosis of retinal disorders.[14,15] The main advantage of OCT is its high scan rate, high resolution, and noncontact character of measurement. Current standard OCT technology used in clinical instruments can be realized

with a broadband light source and a spectrometer (spectral-domain OCT) or with a wavelength-tunable light source and a high-speed point detector (swept source OCT, SS-OCT). Recent advances in tunable lasers and high-speed electronics enabled imaging through the entire length of the eye.[16,17] Apart from visualization of all eye components, the concept of full-eye-length SS-OCT imaging at 1060 nm was demonstrated in ocular biometry, showing high repeatability and reproducibility and very good correlation with other biometers.[18,19] This has led to the introduction of a new generation of optical biometers, such as IOL Master 700 (Carl Zeiss Meditec, Inc., Dublin, CA, USA), Argos (Movu, Inc., Santa Clara, CA, USA), or OA-2000 (Tomey, Nagoya, Japan), enabling improved measuring of cataract patients.[20–22]

Prototype spectral-domain-OCT and SS-OCT anterior segment instruments integrated with air-puff indentation were used to assess biomechanics of the cornea for different IOP levels and to assess biomechanic effects of cross-linking procedures.[12,13] The studies demonstrated mostly the analysis of corneal reaction to air puff in the case of ex vivo model eyes, and limited experiments were reported for human subjects in vivo.[23] Other OCT-based methods to extract corneal biomechanic properties implemented different stimulation scenarios, but it was difficult to apply those approaches in clinical practice.[24–26] Moreover, a limited imaging depth range of the instruments has made the other parts of the eye, such as the anterior chamber (aqueous), the crystalline lens, the vitreous, and the retina, unavailable, and their mutual positions have not been assessed during macroscopic air-puff stimulation.

The aim of this study was to perform an in vivo assessment of the dynamics of all optical components of the eye and the behavior of the eyeball under air-puff conditions by using optical biometry. The comprehensive analysis of deformation processes also included the measurements of intraocular distances, which provide direct access to the response of all ocular elements and media. We wanted to determine the impact of the IOP on the air-puff-induced deformation of the eye. In particular, we checked how the extracted parameters are modified when the IOP is decreased in the eyeballs in in vivo measurements.

Methods

This cross-sectional observational study was approved by the Institutional Ethics Committee at the Nicolaus Copernicus University (Torun, Poland) and adhered to the tenets of the Declaration of Helsinki. Each participant was informed about the nature of the study, and informed consent was obtained prior to the measurements. We recruited 20 Caucasian healthy subjects (mean age, 27.5 ± 3.5 years old; age range, 24–34 years old). The mean spherical equivalent refractive error was −1.1 ± 1.5 D (range, 0 to −5 D), mean K_{ave} was 43.6 ± 1.7 D (range, 40.3–45.8 D), and mean cylinder was −0.93 ± 0.67 D (range, −3.25 to −0.25 D). The protocol excluded subjects with any ocular disorders in the anterior or posterior segment of the eye and previous surgery, candidates with the IOP below 14 mm Hg, people with an allergy to IOP-reducing eye drops, pregnant subjects, or breast-feeding mothers.

We performed a full ophthalmic examination on the eyes of each volunteer, including a visual acuity test, slit-lamp biomicroscopy evaluation (SL 115; Carl Zeiss Meditec AG, Jena, Germany), keratometry (Auto Kerato-Refractometer KR-800; Topcon Corp., Tokyo, Japan), corneal topography (Sirius Scheimpflug Analyzer; Schwind GmbH, Saarbrücken, Germany), and retinal OCT (Avanti RTVue XR; Optovue, Inc., Fremont, CA, USA). One eye of each volunteer was then selected randomly for the study. The measurements of the eye

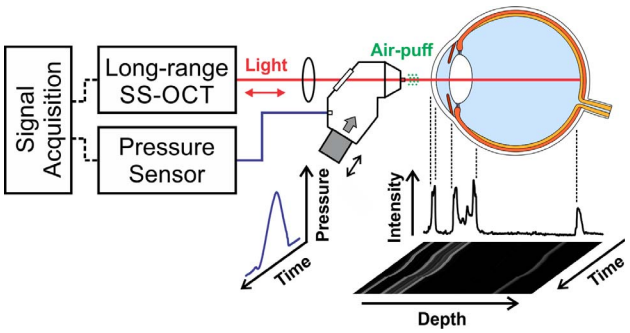

Figure 1. Scheme of the prototype SS-OCT ocular biometer. The system can acquire simultaneously the OCT A-scans in time (M-scan) and corresponding air-puff pressure acting on the cornea. The pressure is later converted into the force based on the sensor calibration.

were performed before and 2 hours after administration of IOP-reducing drops (brimonidine tartrate 0.2%, Alphagan; Allergan, Dublin, Ireland). We used two instruments in each session. The dynamics of all ocular components were measured by a prototype SS-OCT optical biometer integrated with the air-puff (air-puff SS-OCT). The IOP was determined using a GAT device (AT 020; Carl Zeiss Meditec AG, Jena, Germany) mounted to a slit lamp in a sitting position. GAT always followed air-puff SS-OCT to reduce potential impact of the local anesthetic drops (used in applanation tonometry) on the tissue behavior.

The prototype air-puff SS-OCT biometer is shown in Figure 1. The wavelength-tunable light source (OCT swept laser engine; Axsun Technologies, Inc., Billerica, MA, USA) operated at the central wavelength of 1060 nm and at the sweep rate of 30-kA scans/second and enabled achieving imaging depth of 28.03 mm in the air. The optical power illuminating the eye was 1.5 mW, which was below safe exposure limits according to the American National Standard Institute (Z136.1-2007).[27] The axial resolution was 12 μm in the tissue. The mechanic stimulus was provided by an air-puff chamber from a commercial noncontact tonometer (XPert NCT; Reichert, Inc., Depew, NY, USA) integrated in the OCT optical head. The air pulse and the optical probing beam were collinear.[12] The system was able to acquire the optical interference signal (OCT data) as well as the pressure waveform (which was later transformed into the force) generated by the air pulse (Fig. 1). The procedure of conversion pressure into force acting on the cornea was described elsewhere (Grulkowski I, et al. *IOVS* 2018;59:ARVO E-Abstract 279). We implemented lateral scanning of the eye only during preview to enable precise alignment of eye versus optical axis of the instrument. However, no transverse scanning was performed during actual measurement. Because the depth of focus of light illuminating the eye is less than the length of the eye, optimum image quality was obtained when the focal plane was placed at the back of the crystalline lens. The system acquired a series of axial scans at the same location as a function of time (M-scan). Accordingly, the data set (M-scan) consisted of 4000 repeated A-scans (one-dimensional scans) from a single point of the eye (the apex along the visual axis), which corresponded to the total acquisition time of ca. 130 ms with very high temporal resolution (33 μs per axial scan). During each air-puff SS-OCT measurement session, three data sets were acquired.

The SS-OCT instrument was able to reveal the reaction (dynamics) of all ocular components to the air puff. The cornea, the crystalline lens, and the retina were segmented in the M-scan, and the intraocular distances were determined by dividing the optical distances by corresponding group refractive index of the particular eye component: cornea, 1.3755; aqueous, 1.3356; crystalline lens, 1.4048 (averaged); and

Investigative Ophthalmology & Visual Science

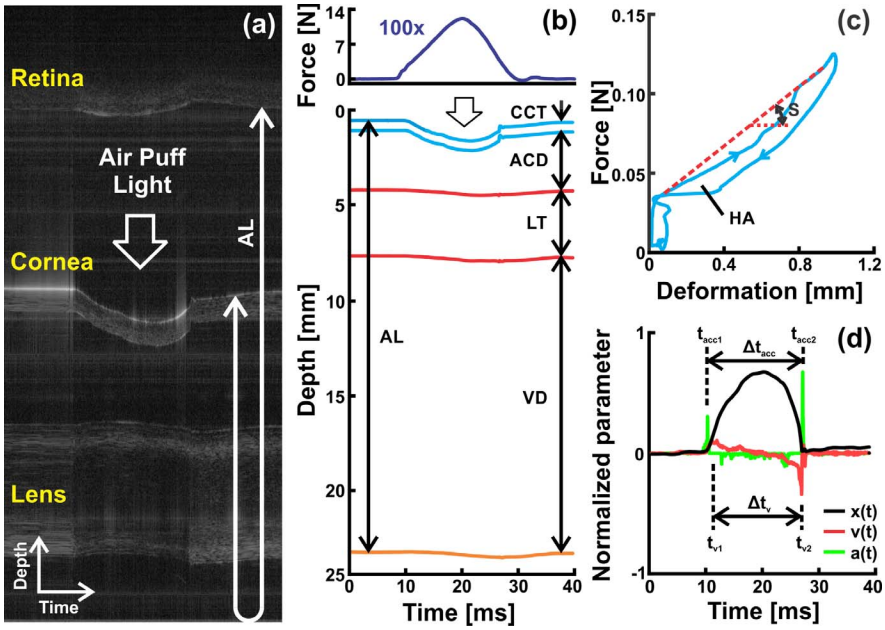

FIGURE 2. Air-pulse-induced dynamics of the ocular components acquired with SS-OCT. Representative data set (right eye of a 23-year-old subject) showing: (**a**) M-scan (axial scans in time); (**b**) segmented interfaces of the cornea, the crystalline lens, and the retina after light refraction correction; (**c**) corneal hysteresis; and (**d**) corneal deformation, speed, and acceleration during air pulse.

vitreous, 1.3354. The methodology of determination of refractive index values used for ocular biometry was presented earlier.[18] Ocular biometry included the measurement of the following intraocular distances: central corneal thickness (CCT), anterior chamber depth (ACD), lens thickness (LT), vitreous depth (VD), and axial length (AL) (Fig. 2). The temporal evolution of the deformations of ocular components was corrected for eye retraction (movement of the whole eyeball during air puff) by using the segmented retinal signal (Grulkowski I, et al. *IOVS* 2018;59:ARVO E-Abstract 279).

We entered all data into a Microsoft Excel 2016 spreadsheet (Microsoft Corp., Redmond, WA, USA). The reproducibility of defined parameters was evaluated using one-way analysis of variance with a random-effects model and expressed with intraclass correlation coefficient (ICC). Pearson correlation coefficient R between extracted parameters and the IOP was calculated, and statistical significance of R was assessed. Statistical significance was taken to be a level of $\alpha = 0.05$. The significance of differences of parameters between the baseline and 2 hours after brimonidine application was also calculated using a paired comparison test. If the differences were not normally distributed (as given by Shapiro-Wilk test), the nonparametric Wilcoxon rank sum test was used.

RESULTS

Figure 2a demonstrates a typical M-scan with 1300 axial scans measured shortly before, during, and after the air-puff excitation was implemented. The full-eye-length M-scan in Figure 2a presents the reaction of the various eye components to the mechanic stimulus. The eye is deformed and returns to its original state. Because of a limited depth range, the retinal signal appears as a complex conjugate in the image.[28] Deformation direction of the cornea and the crystalline lens seem to be opposite, but one has to consider the fact that axial distances in the OCT image are optical. Optical distance is defined as geometric distance multiplied by the refractive index of the medium. The air is optically less thick than the tissue of the same geometric thickness due to the fact that the refractive index of the tissue is higher than that of the air. Accordingly, segmentation of all ocular interfaces and correction for refractive index allowed us to retrieve the geometric intraocular distances and perform true ocular biometry (Fig. 2b). In particular, the intraocular distances were measured at the phase before air puff to correlate the eye biometry with the IOP. Subtracting the intraocular distances measured at the maximum deformation from those measured before air puff enabled determining compression of ocular tissues and media. Moreover, considering the temporal evolution of the pressure (force) and the segmented deformation (Fig. 2b), it was possible to generate the hysteresis loop for the cornea (Fig. 2c). The parameters of the loop, such as hysteresis area (HA) and slope (S), correspond to the biomechanic response of that tissue. Moreover, changes of corneal deformation with time allow for calculation of corneal apex velocity and acceleration, which directly show the dynamics of corneal apex (Fig. 2d). It has to be noted here that negative velocity values mean that the cornea movements during inward and outward applanations have opposite directions.

We were able to extract the biometric changes of the eye at different levels of the IOP, including intraocular distances, deformations of the cornea and the crystalline lens, corneal hysteresis, and characteristic temporal points taken from deformation, its velocity, and acceleration. The Table presents the reproducibility of the identified parameters in a form of the ICC. The highest reproducibility is observed for deformations of all ocular interfaces and corneal HA. Although the times of velocity extrema (t_{v1}, t_{v2}) or acceleration maxima (t_{acc1}, t_{acc2}) have relatively low reproducibility, the time interval $\Delta t_v (= t_{v2} - t_{v1})$ between both velocity extrema and the time interval $\Delta t_{acc} (= t_{acc2} - t_{acc1})$ between both acceleration extrema are characterized by higher reproducibility.

Figure 3 shows the impact of the IOP reduction on selected data that can be extracted from the measurements, for example the deformation of the cornea and the crystalline lens, the hysteresis loop, and the corneal apex velocity, in the eye of a 33-year-old subject. The plots present that the deformation amplitudes and the HA become larger when the IOP is lower.

Table. Reproducibility, Correlation of SS-OCT Parameters With the IOP, and Significance of the Difference of Means for the Entire Population

Parameter	Reproducibility ICC	Pearson Correlation Coefficient Parameter vs. IOP	Mean Difference 2 h vs. 0 h	Significance of Mean Difference 2 h−0 h
IOP	–	**1.0000***	−3.25 ± 1.21 mm Hg	**0.001***
CCT	0.6938	**0.6677***	0.001 ± 0.018 mm	0.420
ACD	0.9842	0.1179	0.000 ± 0.047 mm	0.497
LT	0.9789	−0.0384	0.029 ± 0.059 mm	**0.005***
VD	0.9983	**0.3114***	−0.042 ± 0.061 mm	**0.003***
AL	0.9808	**0.3459***	0.004 ± 0.101 mm	0.139
Cornea deformation	0.8139	**−0.6447***	0.152 ± 0.72 mm	**0.001***
Lens deformation	0.6950	−0.1420	0.034 ± 0.038 mm	**0.001***
Eye retraction	0.7876	−0.1396	−0.014 ± 0.039 mm	0.056
CCT compression	0.1946	0.1832	−0.006 ± 0.020 mm	0.071
ACD compression	0.7395	**0.6002***	−0.119 ± 0.057 mm	**0.001***
LT compression	0.1250	0.1065	−0.003 ± 0.029 mm	0.347
VD compression	0.5066	−0.0600	−0.031 ± 0.037 mm	**0.001***
AL compression	0.1603	**0.2750***	−0.185 ± 0.152 mm	**0.001***
Cornea HA	0.5105	**−0.2289***	(6.0 ± 5.2) × 10^{-6} Nm	**0.001***
Cornea slope S	0.4435	**0.5131***	1.46 ± 0.92 N/mm	**0.001***
t_{v1}	0.2552	**−0.4485***	−0.15 ± 0.71 ms	0.176
t_{v2}	0.4404	**−0.4120***	0.72 ± 0.50 ms	**0.001***
Δt_v	0.6617	**−0.6076***	0.87 ± 0.59 ms	**0.001***
t_{acc1}	0.0217	**0.5697***	−0.15 ± 0.47 ms	0.081
t_{acc2}	0.4083	**−0.3290***	0.72 ± 0.55 ms	**0.001***
Δt_{acc}	0.5368	**−0.5825***	0.88 ± 0.48 ms	**0.001***

Statistical significance is indicated with bold font and asterisk. The abbreviations of parameters are explained in Figure 2.

At the same time, the corneal apex velocity reaches its maximum earlier when the IOP is lower, and the time instance between velocity extrema during inward and outward applanation is longer. What is more, the crystalline lens responds in a different way compared with the cornea. The motion has a form of damped oscillations, which can be described as wobbling (Fig. 3b).

All measured parameters and the results of statistical analysis are tabulated in Supplementary Table S1. A summary of coefficients of correlation between the extracted parameters and the IOP is given in the Table, and correlation plots for some parameters are presented in Figure 4. Statistical significance of Pearson's correlation coefficients is given in Supplementary Table S1. Generally, at baseline there is a statistically significant correlation of CCT (the highest correlation among all parameters achieving 0.67), VD, and AL with IOP, which means that subjects with higher IOP have usually thicker corneas and larger eye balls. The deformation amplitudes of the cornea and the crystalline lens are inversely proportional to the IOP, but the relation is statistically significant only for the cornea. The cornea is deformed more when the IOP is lower. In addition, air-puff-induced compression of eye components shows significant correlation with the IOP in the case of ACD and AL, which is associated with the deformation of the cornea. On the other hand, calculated lens compression values are around zero, suggesting that the entire lens is just shifted during air-puff stimulus application. Finally, the analysis of corneal hysteresis loop, corneal apex velocity, and acceleration demonstrate significant dependence on the IOP. The HA becomes lower, whereas the S increases when the IOP is higher. The time intervals Δt_v and Δt_{acc} inversely proportional to the IOP show relatively high correlation (0.61 and 0.58, respectively).

We also studied the impact of IOP reduction on the change of the extracted parameters. The change of each parameter was defined as the difference between the parameter measured 2 hours after brimonidine application and that parameter measured at the baseline (immediately before brimonidine application). Consequently, this enabled paired comparison and statistical assessment of the differences. The results shown in Figure 5 and summarized in the Table and Supplementary Table S1 indicate that statistically significant reduction of the IOP (–3.25 ± 1.21 mm Hg) was observed 2 hours after administration of brimonidine. Interestingly, the lens became slightly thicker, whereas the vitreous became shallower among

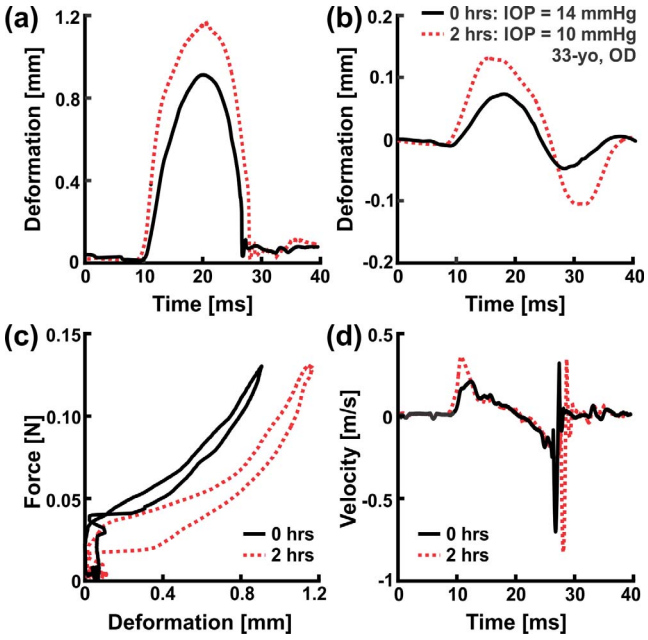

Figure 3. Impact of the IOP reduction on the reaction to the air puff in the case the right eye of 33-year-old subject. Deformation of the cornea in time (**a**), deformation of the crystalline lens in time (lens wobbling) (**b**), hysteresis (**c**), and apex velocity in time (**d**) at the baseline IOP (0 hours) and after IOP reduction (2 hours after brimonidine administration).

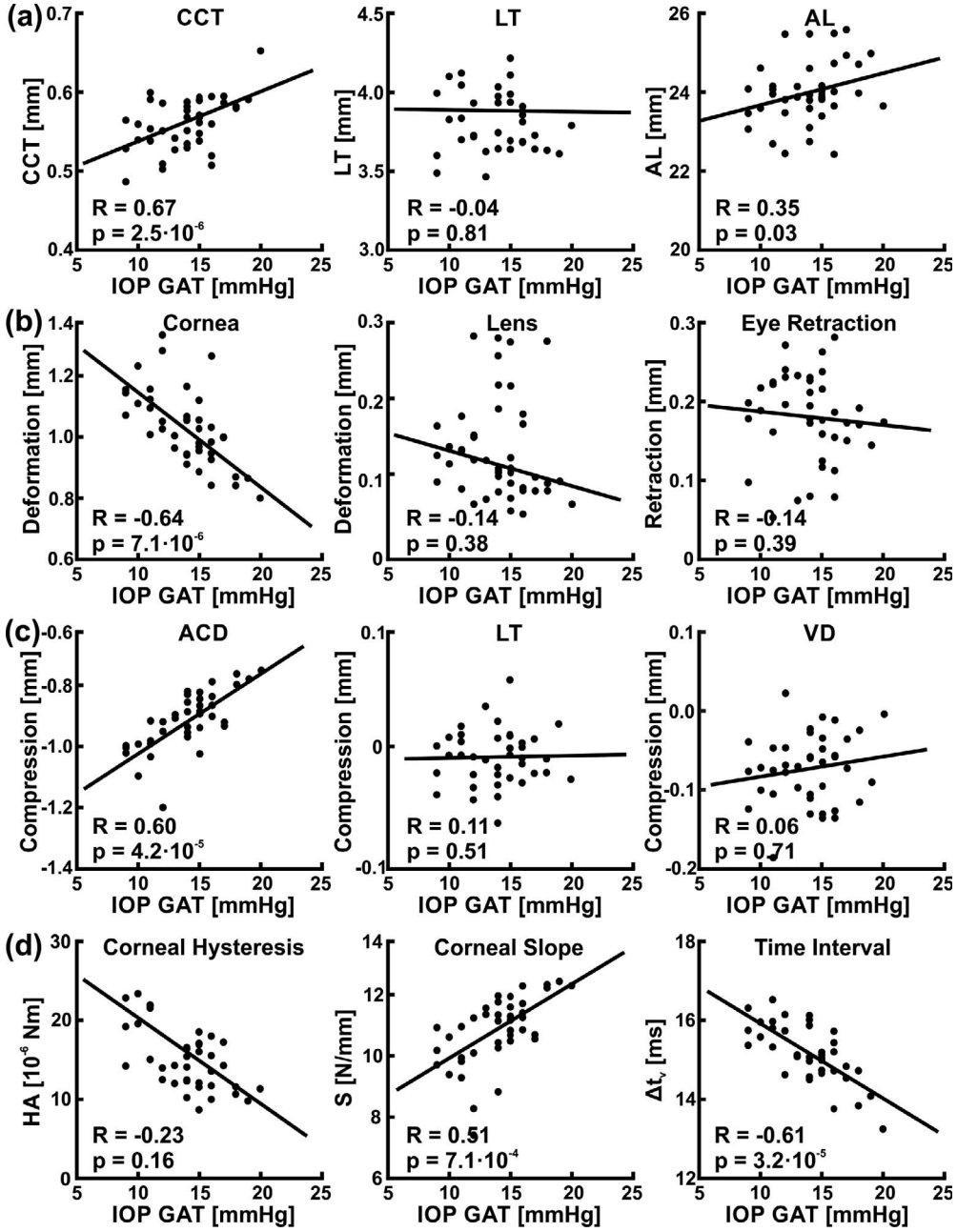

FIGURE 4. Correlation of selected parameters with the IOP: (**a**) baseline ocular biometry, (**b**) deformation amplitude of the cornea and the crystalline lens (wobbling) and eye retraction amplitude extracted from the retinal signal, (**c**) compression of tissues, and (**d**) corneal hysteresis, corneal S, and time interval between extrema of apex velocity. R, Pearson correlation coefficient.

the population when the IOP level was reduced. Data in the Table demonstrate that there is no sufficient evidence that CCT compression, LT compression, and velocity and acceleration maxima during inward applanation phase change when the IOP is reduced. All other parameters indicate statistically significant change during the IOP reduction experiment.

DISCUSSION

The experimental system used in this study combines for the first time two clinically accepted concepts: mechanic stimulus based on a short air-pulse indentation (used in standard noncontact tonometry) and emerging methodology of optical ocular biometry (commercially available in few instruments employing SS-OCT technology).

The features of both techniques provide a unique insight into the dynamics of all ocular components during air puff. First, the system operates at the central wavelength of 1 μm, which characterizes longer light penetration (lower attenuation) and, thus, better performance even in the case of ocular opacifications.[29,30] Second, the possibility to image the eye through its entire length enables visualization of the cornea, the aqueous, the crystalline lens, the vitreous, and the retina during mechanic stimulation at the corneal apex, which is realized by the measurements of intraocular distances. Because previous studies were mainly limited to the analysis of the corneal reaction, the current method represents a compre-

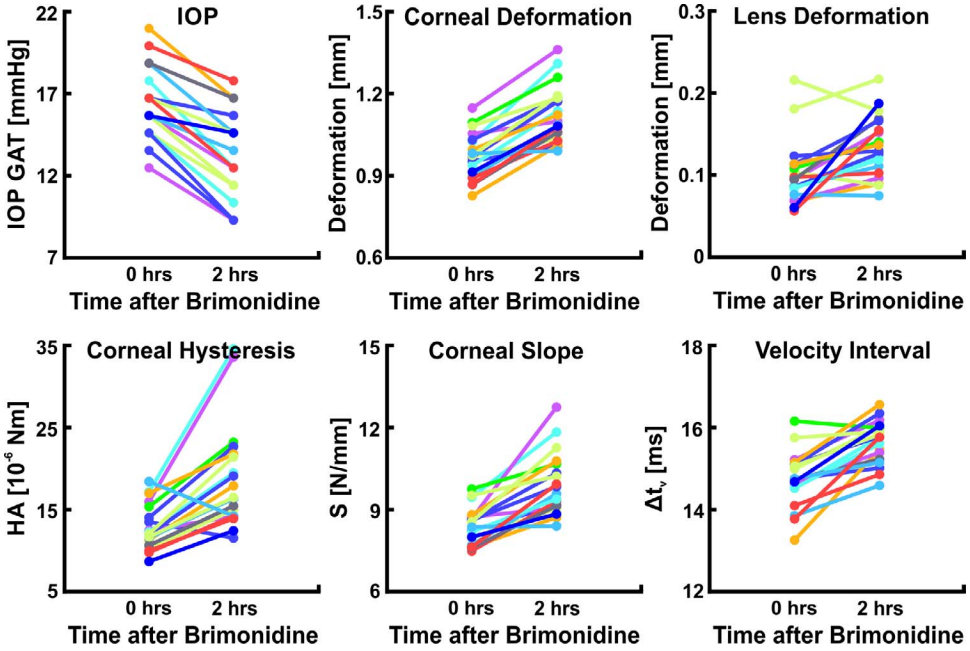

FIGURE 5. Impact of IOP reduction on the selected parameters of eye during air-puff eye deformation. Changes of the parameters in the study group at the baseline (0 hours) and 2 hours after brimonidine administration. All mean differences are statistically significant.

hensive approach to the effect of eye deformation.[12,13] Third, the operation principle of the system is obtained by sacrificing the lateral scanning to have high temporal resolution. The axial scan rate of the SS-OCT setup is more than 10× higher than the frame rate of Scheimpflug camera with air puff (Corvis ST tonometer), although no change in the shape (i.e., the curvature) of the ocular components can be revealed with the proposed approach.[10] Therefore, the acquired data can reveal detailed dynamic reaction of the eye while the air puff is applied. Fourth, the methodology presented in this paper also allows for the extraction of information on whole eye movement (retraction, which also includes head motion in axial direction) during air pulse (Grulkowski I, et al. *IOVS* 2018;59:ARVO E-Abstract 279). Access to eye retraction makes it possible to determine the real deformation of tissues with better reproducibility.[31] Finally, air-puff OCT biometry is noncontact, so topical anesthesia is not required; thus, it improves comfort of a patient.

Ocular biometry with the SS-OCT system showed intersession reproducibility comparable to previously reported laboratory and clinical optical biometers.[18,32,33] The statistical analysis revealed high ICC values for all intraocular distances, which means that SS-OCT can provide reliable biometry measurements. Among all intraocular distances, the lowest ICC was found in corneal thickness, which was due to the axial resolution of the SS-OCT system and limited digital resolution of OCT images (size of the pixel in z-direction, 5 μm), which was also observed in other reports.[18,19,34] Another interesting observation showed that the time intervals Δt_v and Δt_{acc} had higher reproducibility than the times of velocity/acceleration extrema, which may be attributed to the signal processing procedure of identifying those markers in corneal apex velocity/acceleration waveform.

The study design implemented in this project enabled an assessment of the correlations of extracted parameters with the IOP. Intraocular distances measured before air puff associate the axial dimensions of the eyes with different IOP levels. A statistically significant correlation of CCT, VD, and AL indicate that the eyes with higher IOP have thicker corneas, larger vitreous, and longer eye length, which agrees well with the study with glaucoma patients.[35]

The amplitude of corneal deformation is inversely proportional to the IOP, with one of the highest correlation coefficient values among all parameters. When the IOP is higher, the cornea is less deformed, which has been previously confirmed in ex vivo studies with the porcine eyes and can be explained by the increased rigidity of the eye.[36] At the same time, the air puff does not have such a significant effect on the lens deformation because the amplitude is smaller. A closer look at the deformation dynamics of the anterior surface of the crystalline lens reveals a damped oscillatory movement of the lens during application of the air puff. The lens wobbles as the result of its inertia, the impact of adjacent media (aqueous and vitreous), and the biomechanics of suspensory ligament of the lens. This characteristic back-and-forth motion can be observed only due to the correction of deformation for eye retraction (Grulkowski I, et al. *IOVS* 2018;59:ARVO E-Abstract 279). Axial wobbling has been observed for the first time, although the lens wobbling due to lateral eye motion has been experimentally studied using Purkinje imaging.[37]

Air-puff-induced compression of ocular tissues was also quantified by subtraction of intraocular distances measured at two instances: before air puff and at the maximum deformation. The results showed that significant correlation of the compression and the IOP was obtained for ACD and AL, which is the effect of corneal deformation. What is more, the crystalline lens is practically not compressed in the course of the air puff, which indicates that the lens is only displaced during stimulation with air jet.

The proposed system can directly measure the stimulus strength and the reaction of the tissue, which are crucial in understanding the biomechanic properties of the tissue. The observed hysteresis loop indicates tissue viscoelasticity that has been described by the HA. Due to the drop in deformation amplitude, the HA is inversely proportional to the IOP, whereas the hysteresis S showed positive correlation with the IOP.

Statistically significant correlations were also obtained when the corneal deformation waveform was analyzed. The velocity and acceleration showed characteristic extrema (maximum or minimum), which could be associated with both applanation events during air-puff deformation. It is easier to applanate the cornea for lower IOP levels. Therefore, we observed longer intervals between velocity extrema or acceleration extrema when the IOP is lower. The effects were studied using Scheimpflug technology.[38]

The study also aimed at finding the impact of IOP reduction on the extracted parameters. The application of IOP-reducing drug keeps the biomechanics so that we can study a pure effect of IOP. The most prominent effect of brimonidine is 2 hours after application of drops.[39] The direction of changes agrees well with the regression analysis performed earlier. The changes can be regarded as purely associated with the IOP reduction because no effect of brimonidine on anterior segment biometry was reported.[40]

The main limitation of the current study is a relatively low sample size. In addition to that, only healthy volunteers were included in this study. Further measurements can be done with glaucoma patients to confirm the observed effects among this population. Moreover, the instrumentation enabled us to extract information along a single axis only (in our case visual axis). Repeated axial scans forming the M-scan represent one-dimensional information and reveal axial changes in the mutual positions and thickness changes of ocular components. A better control of the dynamic processes after air pulse tissue excitation can be provided, for example with repeated cross-sectional (two-dimensional) imaging, similarly to the Corvis ST device. However, this would require ultrahigh-speed imaging technology, such as SS-OCT with an A-scan rate in the megahertz range.[41] Another disadvantage of this methodology is that the air puff modifies corneal shape significantly (from convex to concave), which affects propagation of light in the eye during the deformation process. Hence, this can be a source of uncertainty especially if the measurement is performed at the point out of the corneal apex. The motion artifacts also contributed to the measurement errors, although the data sets with significant artifacts were discarded immediately after reviewing the data quality so that we could follow with postprocessing of the data.

In conclusion, optical biometry combined with air puff provides comprehensive information on the behavior of all ocular components, including the crystalline lens. While the anterior chamber is deformed, the crystalline lens is displaced and the return looks like axial wobbling. The access to the dynamics of axial length during deformation enables correcting the deformation for eye retraction. As the dynamics of OCT biometry after an air puff change with the reduction of IOP, the technology has the potential not only to provide information on the biomechanics of ocular tissues but also to measure IOP in a noncontact way.

Acknowledgments

Supported by the National Science Center (Grant numbers 2015/18/E/NZ5/00697, 2017/27/B/ST7/00663, and 2017/26/M/NZ5/00849); European Union's Horizon 2020, research, technological development and demonstration programme (BE-OPTICAL; number 675512); European Union's Horizon 2020, Information and Communication Technologies (IMCUSTOMEYE number 779960); and European Union's Horizon 2020, research and innovation programme (CREATE; number 666295).

Disclosure: **E. Maczynska**, None; **J. Rzeszewska-Zamiara**, None; **A. Jimenez Villar**, None; **M. Wojtkowski**, None; **B.J. Kaluzny**, None; **I. Grulkowski**, None

References

1. Kotecha A, White E, Schlottmann PG, Garway-Heath DF. Intraocular pressure measurement precision with the Goldmann applanation, dynamic contour, and ocular response analyzer tonometers. *Ophthalmology*. 2010;117:730–737.
2. Roberts CJ, Liu J, eds. *Corneal Biomechanics: from Theory to Practice*. Amsterdam: Kugler Publications; 2016.
3. Stamper RL. A history of intraocular pressure and its measurement. *Optom Vis Sci*. 2011;88:E16–E28.
4. Whitacre MM, Stein RA, Hassanein K. The effect of corneal thickness on applanation tonometry. *Am J Ophthalmol*. 1993;115:592–596.
5. Kohlhaas M, Boehm AG, Spoerl E, Pürsten A, Grein HJ, Pillunat LE. Effect of central corneal thickness, corneal curvature, and axial length on applanation tonometry. *Arch Ophthalmol*. 2006;124:471–476.
6. Bang SP, Lee CE, Kim YC. Comparison of intraocular pressure as measured by three different non-contact tonometers and goldmann applanation tonometer for non-glaucomatous subjects. *BMC Ophthalmol*. 2017;17:199.
7. Luce DA. Determining in vivo biomechanical properties of the cornea with an ocular response analyzer. *J Cataract Refract Surg*. 2005;31:156–162.
8. Shah S, Laiquzzaman M, Cunliffe I, Mantry S. The use of the Reichert ocular response analyser to establish the relationship between ocular hysteresis, corneal resistance factor and central corneal thickness in normal eyes. *Cont Lens Ant Eye*. 2006;29:257–262.
9. Koprowski R, Wilczynski S, Nowinska A, et al. Quantitative assessment of responses of the eyeball based on data from the Corvis tonometer. *Comput Biol Med*. 2015;58:91–100.
10. Hong J, Xu J, Wei A, et al. A new tonometer—the Corvis ST tonometer: clinical comparison with noncontact and goldmann applanation tonometers. *Invest Ophthalmol Vis Sci*. 2013;54:659–665.
11. Reznicek L, Muth D, Kampik A, Neubauer AS, Hirneiss C. Evaluation of a novel Scheimpflug-based non-contact tonometer in healthy subjects and patients with ocular hypertension and glaucoma. *Br J Ophthalmol*. 2013;97:1410–1414.
12. Alonso-Caneiro D, Karnowski K, Kaluzny BJ, Kowalczyk A, Wojtkowski M. Assessment of corneal dynamics with high-speed swept source optical coherence tomography combined with an air puff system. *Opt Express*. 2011;19:14188–14199.
13. Dorronsoro C, Pascual D, Perez-Merino P, Kling S, Marcos S. Dynamic OCT measurement of corneal deformation by an air puff in normal and cross-linked corneas. *Biomed Opt Express*. 2012;3:473–487.
14. Swanson EA, Fujimoto JG. The ecosystem that powered the translation of OCT from fundamental research to clinical and commercial impact [Invited]. *Biomed Opt Express*. 2017;8:1638–1664.
15. de Boer JF, Leitgeb R, Wojtkowski M. Twenty-five years of optical coherence tomography: the paradigm shift in sensitivity and speed provided by Fourier domain OCT [Invited]. *Biomed Opt Express*. 2017;8:3248–3280.
16. Grulkowski I, Liu JJ, Potsaid B, et al. Retinal, anterior segment and full eye imaging using ultrahigh speed swept source OCT with vertical-cavity surface emitting lasers. *Biomed Opt Express*. 2012;3:2733–2751.
17. Klein T, Huber R. High-speed OCT light sources and systems [Invited]. *Biomed Opt Express*. 2017;8:828–859.
18. Grulkowski I, Liu JJ, Zhang JY, et al. Reproducibility of a long-range swept-source optical coherence tomography ocular biometry system and comparison with clinical biometers. *Ophthalmology*. 2013;120:2184–2190.
19. Grulkowski I, Manzanera S, Cwiklinski L, Sobczuk F, Karnowski K, Artal P. Swept source optical coherence

tomography and tunable lens technology for comprehensive imaging and biometry of the whole eye. *Optica*. 2018;5:52–59.

20. Hoffer KJ, Hoffmann PC, Savini G. Comparison of a new optical biometer using swept-source optical coherence tomography and a biometer using optical low-coherence reflectometry. *J Cataract Refract Surg*. 2016;42:1165–1172.
21. Huang J, Savini G, Hoffer KJ, et al. Repeatability and interobserver reproducibility of a new optical biometer based on swept-source optical coherence tomography and comparison with IOLMaster. *Br J Ophthalmol*. 2016;101:493–498.
22. Srivannaboon S, Chirapapaisan C, Chonpimai P, Loket S. Clinical comparison of a new swept-source optical coherence tomography–based optical biometer and a time-domain optical coherence tomography–based optical biometer. *J Cataract Refract Surg*. 2015;41:2224–2232.
23. Maczynska E, Karnowski K, Szulzycki K, et al. Assessment of the influence of viscoelasticity of cornea in animal ex vivo model using air-puff optical coherence tomography and corneal hysteresis. *J Biophotonics*. 2018;12:e201800154.
24. Larin KV, Sampson DD. Optical coherence elastography: OCT at work in tissue biomechanics [Invited]. *Biomed Opt Express*. 2017;8:1172–1202.
25. Akca BI, Chang EW, Kling S, et al. Observation of sound-induced corneal vibrational modes by optical coherence tomography. *Biomed Opt Express*. 2015;6:3313–3319.
26. Kirby MA, Pelivanov I, Song S, et al. Optical coherence elastography in ophthalmology. *J Biomed Opt*. 2017;22:121720.
27. Delori FC, Webb RH, Sliney DH. Maximum permissible exposures for ocular safety (ANSI 2000), with emphasis on ophthalmic devices. *J Opt Soc Am A-Opt Image Sci Vis*. 2007;24:1250–1265.
28. Wojtkowski M, Kowalczyk A, Leitgeb R, Fercher AF. Full range complex spectral optical coherence tomography technique in eye imaging. *Opt Lett*. 2002;27:1415–1417.
29. Wang W, Miao Y, Savini G, et al. Precision of a new ocular biometer in eyes with cataract using swept source optical coherence tomography combined with placido-disk corneal topography. *Sci Rep*. 2017;7:13736.
30. Hirnschall N, Varsits R, Doeller B, Findl O. Enhanced penetration for axial length measurement of eyes with dense cataracts using swept source optical coherence tomography: a consecutive observational study. *Ophthalmol Ther*. 2018;7:119–124.
31. Boszczyk A, Kasprzak H, Jozwik A. Eye retraction and rotation during Corvis ST "air puff" intraocular pressure measurement and its quantitative analysis. *Ophthalmic Physiol Opt*. 2017;37:253–262.
32. Vogel A, Dick HB, Krummenauer F. Reproducibility of optical biometry using partial coherence interferometry: intraobserver and interobserver reliability. *J Cataract Refract Surg*. 2001;27:1961–1968.
33. Buckhurst PJ, Wolffsohn JS, Shah S, Naroo SA, Davies LN, Berrow EJ. A new optical low coherence reflectometry device for ocular biometry in cataract patients. *Br J Ophthalmol*. 2009;93:949–953.
34. Grulkowski I, Liu JJ, Potsaid B, et al. High-precision, high-accuracy ultralong-range swept-source optical coherence tomography using vertical cavity surface emitting laser light source. *Opt Lett*. 2013;38:673–675.
35. Leydolt C, Findl O, Drexler W. Effects of change in intraocular pressure on axial eye length and lens position. *Eye*. 2007;22:657–661.
36. Pallikaris IG, Kymionis GD, Ginis HS, Kounis GA, Tsilimbaris MK. Ocular rigidity in living human eyes. *Invest Ophthalmol Vis Sci*. 2005;46:409–414.
37. Tabernero J, Artal P. Lens oscillations in the human eye. implications for post-saccadic suppression of vision. *PLoS One*. 2014;9:e95764.
38. Tian L, Wang D, Wu Y, et al. Corneal biomechanical characteristics measured by the CorVis Scheimpflug technology in eyes with primary open-angle glaucoma and normal eyes. *Acta Ophthalmol*. 2016;94:e317–e324.
39. van der Valk R, Webers CAB, Schouten JSAG, Zeegers MP, Hendrikse F, Prins MH. Intraocular pressure–lowering effects of all commonly used glaucoma drugs: a meta-analysis of randomized clinical trials. *Ophthalmology*. 2005;112:1177–1185.
40. Marchini G, Babighian S, Tosi R, Bonomi L. Effects of 0.2% brimonidine on ocular anterior structures. *J Ocul Pharmacol Ther*. 1999;15:337–344.
41. Singh M, Han Z, Nair A, Schill A, Twa MD, Larin KV. Applanation optical coherence elastography: noncontact measurement of intraocular pressure, corneal biomechanical properties, and corneal geometry with a single instrument. *J Biomed Opt*. 2017;22:20502.

Investigative Ophthalmology & Visual Science